

# A Robust Deep Learning Method with Uncertainty Estimation for the Pathological Classification of Renal Cell Carcinoma based on CT Images

Ni Yao<sup>1</sup> · Hang Hu<sup>1</sup> · Kaicong Chen<sup>2</sup> · Chen Zhao<sup>3</sup> · Yuan Guo<sup>5</sup> · Boya Li<sup>2</sup> · Jiaofen Nan<sup>1</sup> · Yanting Li<sup>1</sup> · Chuang Han<sup>1</sup> · Fubao Zhu<sup>1</sup> · Weihua Zhou<sup>3,4\*</sup> · Li Tian<sup>2\*</sup>

<sup>1</sup> School of Computer and Communication Engineering, Zhengzhou University of Light Industry, Zhengzhou 450002, Henan, China

<sup>2</sup> Department of Medical Imaging, State Key Laboratory of Oncology in South China, Guangdong Provincial Clinical Research Center for Cancer, Collaborative Innovation Center for Cancer Medicine, Sun Yat-Sen University Cancer Center, Guangzhou, 510060, Guangdong, China

<sup>3</sup> Department of Applied Computing, Michigan Technological University, Houghton, MI, USA

<sup>4</sup> Center for Biocomputing and Digital Health, Institute of Computing and Cybersystems, and Health Research Institute, Michigan Technological University, Houghton, MI, USA

<sup>5</sup> Department of Radiology, the First People's Hospital of Guangzhou, Guangzhou, 510180, Guangdong, China

\*Correspondence:

Li Tian

[tianli@sysucc.org.cn](mailto:tianli@sysucc.org.cn)

Weihua Zhou

[whzhou@mtu.edu](mailto:whzhou@mtu.edu)

## Abstract

**Objectives** To develop and validate a deep learning-based diagnostic model incorporating uncertainty estimation so as to facilitate radiologists in the preoperative differentiation of the pathological subtypes of renal cell carcinoma (RCC) based on CT images.

**Methods** Data from 668 consecutive patients, pathologically proven RCC, were retrospectively collected from Center 1. By using five-fold cross-validation, a deep learning model incorporating uncertainty estimation was developed to classify RCC subtypes into clear cell RCC (ccRCC), papillary RCC (pRCC), and chromophobe RCC (chRCC). An external validation set of 78 patients from Center 2 further evaluated the model's performance.

**Results** In the five-fold cross-validation, the model's area under the receiver operating characteristic curve (AUC) for the classification of ccRCC, pRCC, and chRCC was 0.868 (95% CI: 0.826-0.923), 0.846 (95% CI: 0.812-0.886), and 0.839 (95% CI: 0.802-0.88), respectively. In the external validation set, the AUCs were 0.856 (95% CI: 0.838-0.882), 0.787 (95% CI: 0.757-0.818), and 0.793 (95% CI: 0.758-0.831) for ccRCC, pRCC, and chRCC, respectively.

**Conclusions** The developed deep learning model demonstrated robust performance in predicting the pathological subtypes of RCC, while the incorporated uncertainty emphasized the importance of understanding model confidence, which is crucial for assisting clinical decision-making for patients with renal tumors.

**Clinical relevance statement** Our deep learning approach, integrated with uncertainty estimation, offers clinicians a dual advantage: accurate RCC subtype predictions complemented by diagnostic

confidence references, promoting informed decision-making for patients with RCC.

**Key Points:**

- Incorporation of uncertainty into deep learning models improves the interpretability and reliability in RCC subtypes classification compared to conventional methods.
- Our experimental results demonstrate that the rate of correct predictions increases as the uncertainty grade of a prediction decreases, confirming its diagnostic performance.
- Radiologists are provided with classification diagnoses and their associated uncertainty, enhancing the transparency and trustworthiness of the AI model in medical imaging applications.

**Keywords** Deep learning · Renal cell carcinoma · Pathological classification · Computed Tomography

**Abbreviations**

AUC	Area under the receiver operating characteristic curve
ccRCC	Clear cell renal cell carcinoma
chRCC	Chromophobe renal cell carcinoma
CI	Confidence interval
CMP	Corticomedullary phase
CNN	Convolutional neural network
CT	Computed tomography
NP	Nephrographic phase
PCP	Precontrast phase
pRCC	Papillary renal cell carcinoma
RCC	Renal cell carcinoma
ROC	Receiver operating characteristic
ROI	Region of interest
VOI	Volume of interest

## Introduction

Renal cell carcinoma (RCC) accounts for approximately 90-95% of renal cancers[1], and is often classified into several histologic subtypes based on their morphological characteristics. The most common is clear cell RCC (ccRCC), accounting for 75% of the cases. This subtype is notably aggressive with a less favorable prognosis. Following ccRCC, the second and third most frequent subtypes are papillary RCC (pRCC) and chromophobe RCC (chRCC), making up 10-15% and 5% of the cases respectively[2]. The RCC subtypes range from indolent to aggressive, each with associated treatment considerations[3]. In addition, the selection of targeted drug therapy and immunotherapy for advanced tumors is also based on the RCC subtypes[4, 5]. Consequently, accurate pathological classification is crucial for patients with RCC in both prognosis and therapeutic strategies[6].

Percutaneous renal biopsy provides diagnostic value in classifying the most common types of RCC[7]. However, the biopsy is invasive, associated with complications, and may be limited by tumor location and the optimal timing for the procedure. Growing evidence suggests that Computed Tomography (CT) plays a crucial role over the course of RCC treatment, from diagnosing and staging the disease to assessing the response to treatment[8]. However, significant overlaps exist in image-level features between renal tumor subtypes, which complicates subtype classification and introduces inter-observer variability[9]. These clinical challenges point to the need for automated systems to reduce misdiagnosis costs and assist radiologists in medical image interpretation[10].

In recent years, deep learning based on convolutional neural network (CNN) has shown potential in enhancing the efficiency of radiologists for complex medical image analysis, especially in the field of RCC[11-13]. Specifically, deep learning has been primarily applied to medical image detection and segmentation[14-16]. It has also been dedicated to purposeful classification tasks, such as distinguishing between benign and malignant tumors and performing differential diagnosis of the histological subtypes of RCC[17, 18]. However, the automation level and accuracy of these approaches need to be improved. In addition, compared to accuracy, sensitivity, specificity, receiver operating characteristic (ROC) curve, and area under ROC curve (AUC), researchers rarely provide uncertainty estimation in their outputs. Uncertainty provides a measure of reliability for the model's predictions, allowing people to determine the model's confidence in its classification decisions more clearly. Therefore, from an evidence-based medicine perspective, our goal is not only to develop an efficient diagnostic model, but also to pay more attention to ensuring that the model can sensitively identify difficult cases and reduce the workload of radiologists.

Against the above background, we aimed to propose a framework for the automatic pathological classification of RCC based on CT images by combining uncertainty estimation and deep learning, including a target detection model specifically designed to identify areas of renal tumors and a classification model to distinguish three major pathological subtypes of RCC.

## Materials and methods

### Study population

This retrospective study was approved by the Ethics Committee of both the Sun Yat-sen University Cancer Center and the First People's Hospital of Guangzhou, with informed consent waived for all patients.

We reviewed medical records from January 2016 to November 2022 at the Sun Yat-sen University Cancer Center (Center 1) and from February 2017 to June 2023 at the First People's Hospital of Guangzhou (Center 2). The patients included had histopathologically confirmed diagnoses of ccRCC, pRCC, or chRCC (Fig. 1). The following criteria applied to data exclusion: (1) incomplete 4-phase CT scanning (unenhanced, corticomedullary, nephrographic, and excretory phases); (2) poor image quality (such as motion artifacts, metal artifacts); and (3) the presence of ambiguous or contradicting clinical data. Finally, 668 consecutive patients from Center 1 (ccRCC n=395, pRCC n=167, chRCC n=106) and 78 from Center 2 (ccRCC n=49, pRCC n=11, chRCC n=17) were included.

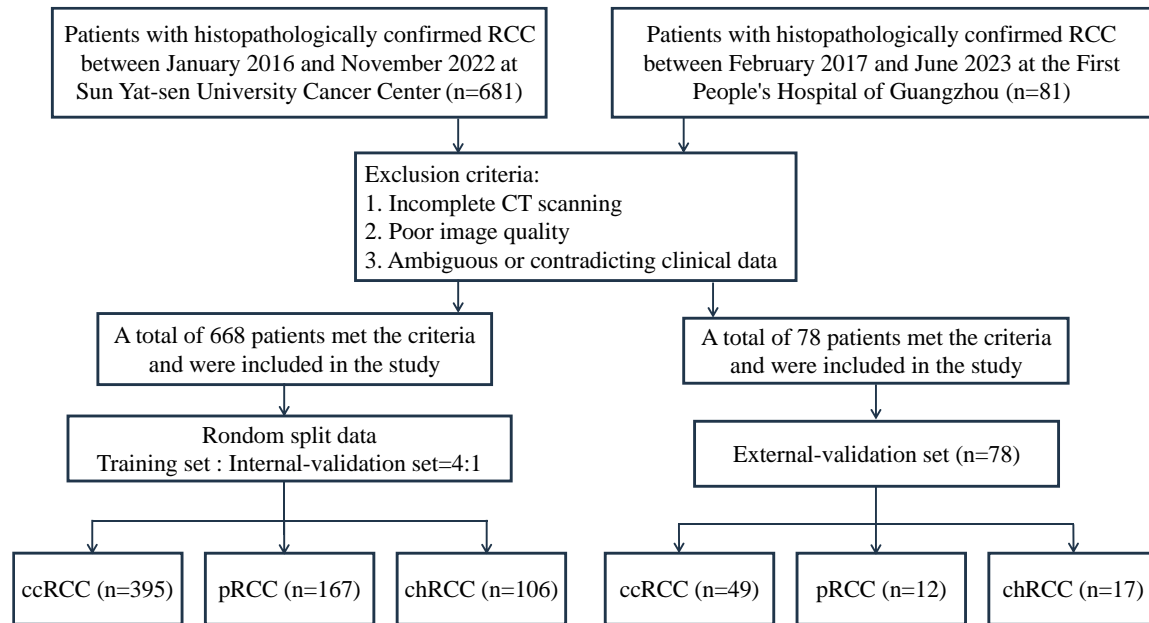


**Fig. 1** Flowchart of patient recruitment. *ccRCC*, clear cell renal cell carcinoma; *pRCC*, papillary renal cell carcinoma; *chRCC*, chromophobe renal cell carcinoma

### CT Image Acquisition

All patients underwent CT examination using multi-slice spiral CT scanners (Center 1: Somatom Force, Siemens Healthineers, Forchheim, Germany; Center 2: Aquilion 64, Toshiba, Tokyo, Japan). Data acquisition was performed in 3 phases: the precontrast phase (PCP), the corticomedullary phase (CMP; 30-second delay after contrast injection), and the nephrographic phase (NP; 90-second delay after contrast injection). After the unenhanced scan, an intravenous bolus injection of nonionic contrast media (350 mg/mL; 1.5 mL/kg) was administered at a rate of 4 mL/s.

### Data Preprocessing

The CT slices for each patient were processed to better analyze the renal parenchyma areas, with the window width and level set to 300 and 40, respectively. The CT scans were then resampled using three spline interpolations to obtain uniform  $1 \times 1 \times 1 \text{ mm}^3$  voxel images. The pixel values were then normalized to the range of 0 to 1, standardizing the data across the entire dataset in preparation for the subsequent tumor detection phase.

### **Tumor detection and image cropping**

We utilized an automated method to detect tumor regions in our dataset. This method allows the model to concentrate on the CT images regions of interest (ROIs), reducing noise for the subsequent classification of subtypes. A YOLO object detection model was built using the Pytorch 1.7 framework and Python 3 language. This model was trained and validated on the publicly available KiTS19 dataset, which provides renal tumor segmentation labels. The segmentation labels were converted to YOLO format that includes the bounding box center coordinates and the box's relative dimensions for each CT slice. Throughout the detection process, we applied data augmentation techniques to enhance the model's generalization capabilities.

Using this trained model, tumor regions in the CT images were automatically detected. CT slices without any kidney tumors (those where the model detected none) were excluded from further analysis. The model achieved an average precision of 0.87 at mean intersection over union=0.5. After detection, we conducted post-processing on the results to expand 1.2 times the dimensions of the detected bounding boxes, starting from the top-left corner, ensuring complete tumor capture along with its surrounding context in the cropped images. The detection results for each 2D slice were integrated to identify the tumor's maximum range in the three-dimensional space, ensuring the comprehensive inclusion of all tumor regions. Using the derived 3D boundaries of the tumor, the corresponding volumes of interest (VOIs) were cropped from the original CT data for the subsequent subtype classification. These cropped regions were then reviewed by a trained technician for validation. Ambiguous cases were referred to an experienced radiologist for consultation. After establishing the accuracy and consistency of these cropped images, they were processed in readiness for the impending classification.

### **Deep learning model development**

Our classification model is a 3D CNN adapted from the architecture proposed by Wang et al[19]. This model incorporates two residual blocks designed for efficient feature extraction and gradient propagation. Following the initial preprocessing and cropping of volumes, these VOIs are fed into our network. Each convolutional layer contains multiple channels to extract distinct features from the input, preserving the spatial information from the CT volume. Instead of using a softmax layer as in conventional classification models, our architecture outputs non-negative continuous values. These values are treated as evidence, which provides a basis for the parameters of a Dirichlet distribution in our evidence-based uncertainty estimation[20].

The structure of the renal cell carcinoma subtype classification network is shown in Fig. 1. The model was trained using the PyTorch library on a Tesla V100 GPU with 32 GB GPU memory. During the training phase, optimization was performed using the adaptive moment optimizer at a learning rate of 0.0001. The batch sizes of the models were set to 32, and the number of training epochs was set to 300. The detailed network structure can be seen in Fig. 2.

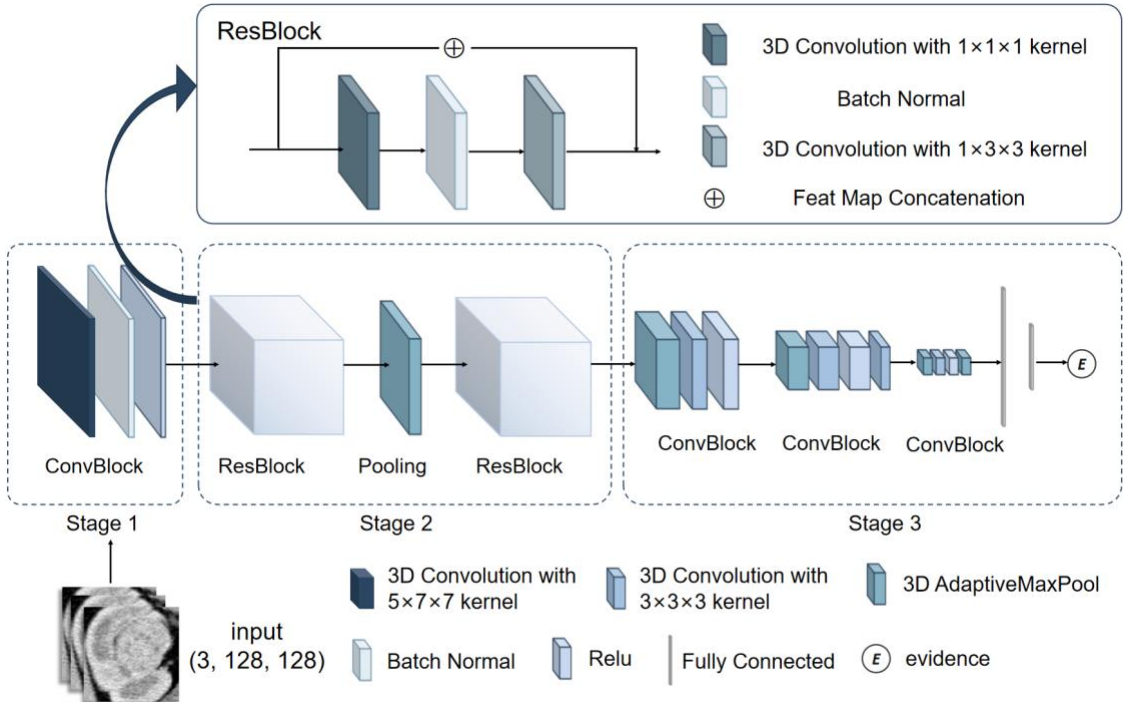


**Fig. 2** Structure of the 3D convolutional neural network for renal cell carcinoma subtype classification. Stage 1: 3D convolutional block layer; Stage 2: two 3D residual blocks with a pooling layer; Stage 3: output layer producing non-negative values for uncertainty estimation

### Uncertainty Estimation and Loss Function

To quantify the uncertainty in our model predictions, we employed an approach based on the Dirichlet distribution. Central to this method is the translation of our model's outputs, which we term as evidence, into parameters for the Dirichlet distribution. The Dirichlet distribution relies on strictly positive parameters to meaningfully represent the strength or support for different classes. To achieve this, especially when the obtained evidence from our model is approach zero, we add a constant of 1 to the evidence. Building on this foundation, the uncertainty  $u$  is quantified by the equation:

$$u = \frac{K}{\sum_{j=1}^K (e_j + 1)}$$

$e_j$  corresponds to the evidence associated with the  $j$ -th class.  $K$  representing the total number of classes, serves to normalize the uncertainty measure, ensuring that it remains proportionate and avoids inflate with an increase in the number of classes.

Another crucial component of our uncertainty estimation involves the design of the loss function. The selected loss function serves a dual purpose: it aligns the model's output with the Dirichlet distribution for uncertainty estimation while addressing and mitigating issues related to class imbalances. Class imbalances arise when certain classes have considerably fewer samples than others, potentially causing the model to exhibit a bias toward predicting classes with larger sample sizes. In our datasets, there is a notable imbalance with a greater number of ccRCC samples compared to the other two classes, and we should address this imbalance appropriately. Let  $y_j$  represent the one-hot encoding of the labels. The loss function can be expressed as:

$$L_i = \sum_{j=1}^K y_{ij} \left( \psi \left( \sum_{j=1}^K (e_j + 1) \right) - \psi(e_{ij} + 1) \right) w_j$$

The  $w_j$  represents the weight for the  $j$ -th class in the loss function. In this method, it is chosen to be the reciprocal of the number of samples for its respective class. The function  $\psi(\cdot)$  is the logarithmic derivative of the gamma function, transforming the model's outputs into probabilistic estimates, thereby facilitating the expression of prediction uncertainty.

### Evaluation

The evaluation metrics consisted of two parts: the evaluation metrics of RCC subtyping, and the metrics to analyze the effectiveness of introduced uncertainty grades.

The primary classification evaluation metric for both internal and external datasets was the AUC of the ROC curve, assessing accuracy, sensitivity, and specificity. AUC values from five-fold cross-validation were presented with 95% confidence intervals (CI).

Given that the range of uncertainty spans from 0 to 1, we evenly distributed this range to define five uncertainty grades. To evaluate the effectiveness of incorporating uncertainty into the model, the correct rate for each grade was calculated based on the number of accurate predictions relative to the total number of predictions within that specific grade.

The statistical analyses were performed in Python 3.7. The ROC curves were plotted and the AUCs were calculated based on scikit-learn library.

## Results

### Population

Table 1 details the demographics and kidney tumor subtype distribution for 745 patients (mean age  $53.3 \pm 12.5$  years) used in our study. The datasets were sourced from Sun Yat-sen University Cancer Center (training and internal validation sets) and the First People's Hospital of Guangzhou (external validation set). In these datasets, the distribution of RCC subtypes remained consistent, with ccRCC being predominant. The overall tumor diameter was  $53.8 \pm 30.3$  mm; more specifically, the diameters for the subtypes were  $51.9 \pm 28.3$  mm for ccRCC,  $61.2 \pm 36.9$  mm for pRCC, and  $54.1 \pm 30.2$  mm for chRCC.

**Table 1** Patient characteristics and tumor size distribution on training and validation sets

Characteristic	All	Training dataset	Internal validation dataset	External validation dataset
Patients, <i>n</i>	746	534	134	78
Age, <i>n</i> (%)				
<40	117 (16)	92 (21)	22 (16)	3 (4)
40-60	421 (56)	295 (68)	74 (55)	52 (67)
>60	208 (28)	147 (11)	38 (28)	23 (29)
Gender, <i>n</i> (%)				
Female	260 (35)	181 (34)	51 (38)	28 (36)
Male	486 (65)	353 (66)	83 (62)	50 (64)
Subtype, <i>n</i> (%)				
ccRCC	444 (59)	316 (59)	79 (59)	49 (63)
pRCC	118 (16)	85 (16)	21 (16)	12 (15)
chRCC	184 (25)	133 (25)	34 (25)	17 (22)
Maximum tumor diameter (mm)				
<30	151 (20)	111 (21)	26 (19)	14 (18)
30-50	252 (34)	185 (34)	39 (29)	28 (36)
50-70	168 (23)	112 (21)	34 (25)	22 (28)
>70	175 (23)	126 (24)	35 (26)	14 (18)

\*The training and internal validation datasets are from fold 1 in the five-fold cross-validation procedure. ccRCC, clear cell renal cell carcinoma; pRCC, papillary renal cell carcinoma; chRCC, chromophobe renal cell carcinoma

### Classification Performance on Validation Sets

In the internal validation dataset, the deep learning model achieved AUCs of  $0.874 \pm 0.039$  for ccRCC,  $0.849 \pm 0.03$  for pRCC, and  $0.841 \pm 0.031$  for chRCC. In the external validation set, the AUCs were  $0.860 \pm 0.018$ ,  $0.787 \pm 0.025$ , and  $0.795 \pm 0.029$  for ccRCC, pRCC, and chRCC, respectively. Fig. 3 presents the ROC curves for each RCC subtype, based on the model's discrimination for each classification. These curves represent outcomes from the five-fold cross-validation, showcasing the model's performance across different partitions of the dataset.

Additional performance metrics, including accuracy, sensitivity, and specificity for each subtype,

are detailed in Table 2. These metrics further provide insight into the model's ability to differentiate RCC subtypes across the internal and external datasets.

**Table 2** The performance of the model in classifying renal cell carcinoma subtype classification on internal and external validation sets

		Accuracy	Sensitivity	Specificity	AUC
Internal Validation Set	ccRCC	0.791±0.016	0.828±0.082	0.736±0.111	0.874±0.039
	pRCC	0.871±0.024	0.566±0.042	0.929±0.032	0.849±0.030
	chRCC	0.815±0.030	0.634±0.106	0.874±0.064	0.841±0.031
External Validation Set	ccRCC	0.763±0.028	0.727±0.043	0.829±0.064	0.860±0.018
	pRCC	0.826±0.040	0.600±0.050	0.864±0.043	0.787±0.025
	chRCC	0.771±0.027	0.600±0.097	0.820±0.046	0.795±0.029

\*The data are reported as the mean±SD based on five-fold cross-validation SD standard deviation. *ccRCC*, clear cell renal cell carcinoma; *pRCC*, papillary renal cell carcinoma; *chRCC*, chromophobe renal cell carcinoma; *AUC*, area under the curve.

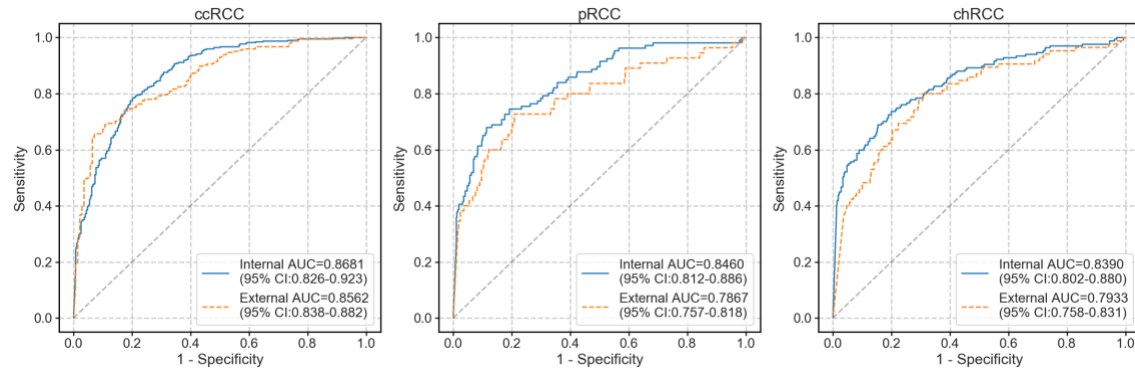


**Fig. 3** The area under the receiver operating characteristic curve (AUC) of five-fold cross-validation in internal and external sets. *ccRCC*, clear cell renal cell carcinoma; *pRCC*, papillary renal cell carcinoma; *chRCC*, chromophobe renal cell carcinoma; *CI*, confidence interval

### Uncertainty Analysis

In our deep learning model, uncertainty estimation was crucial for assessing the reliability of subtype predictions. This evaluation was based on the best model obtained through five-fold cross-validation.

For the internal validation set, the median uncertainties were 0.24 for ccRCC, 0.22 for pRCC, and 0.19 for chRCC. These values were slightly higher for the external validation set: 0.26 for ccRCC, 0.24 for pRCC, and 0.23 for chRCC. Fig. 4 displays the uncertainty grades and their correlation with correct rates for both validation sets. Overall, as the uncertainty grade decreases, the rate of accurate predictions tends to increase. Fig. 5 contrasts the overall correct rate between the two validation sets across varying uncertainty grades. At grade 1, the internal validation set achieved a correct rate of 89.29% (n=134), and the external validation set was at 77.78% (n=78). Predictions with high uncertainty grades (4-5, n=5) showed an 80% wrong rate, which indicates the importance of uncertainty in identifying potentially challenging diagnostic scenarios. Several anomalous cases are illustrated in Fig. 6.

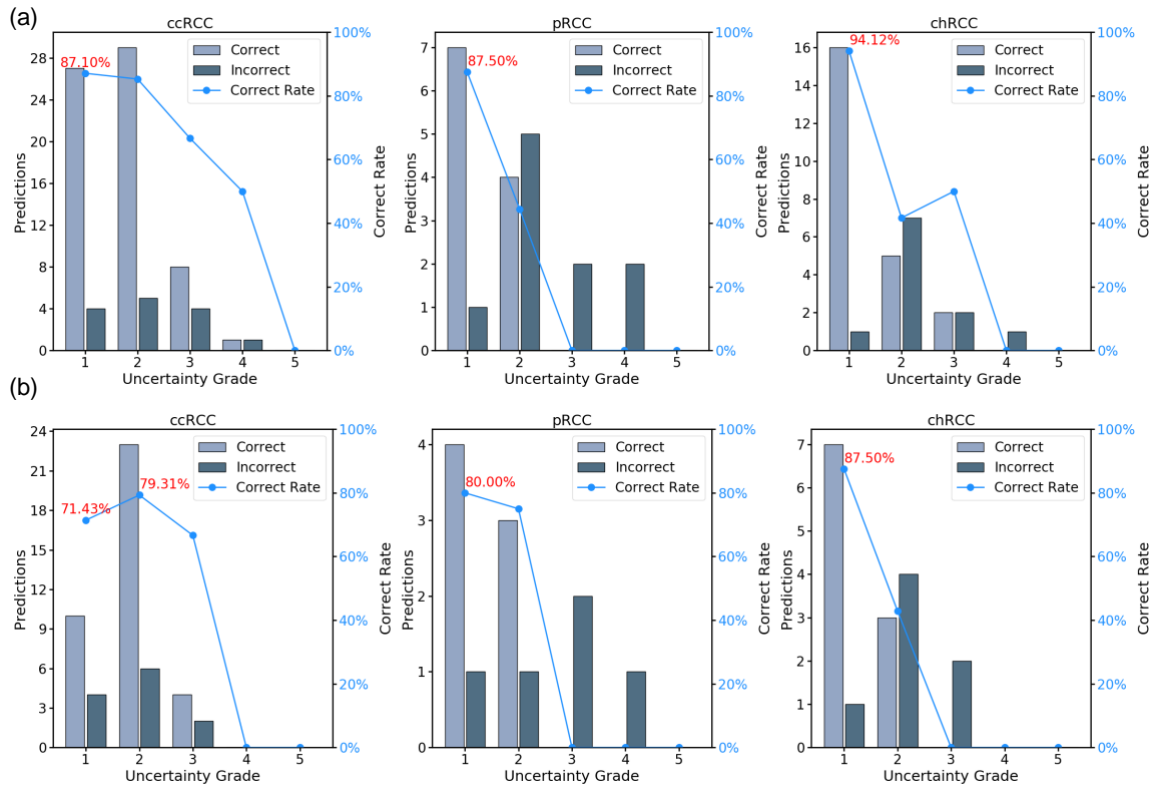


**Fig. 4** Uncertainty-graded prediction performance for kidney cancer subtypes: (a) internal validation set and (b) external validation set. *ccRCC*, clear cell renal cell carcinoma; *pRCC*, papillary renal cell carcinoma; *chRCC*, chromophobe renal cell carcinoma

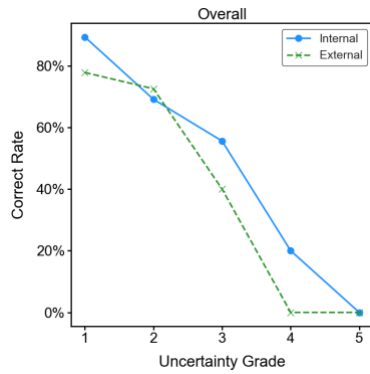


**Fig. 5** Comprehensive correct rate comparison of all subtypes on internal and external validation sets for different grades of uncertainty

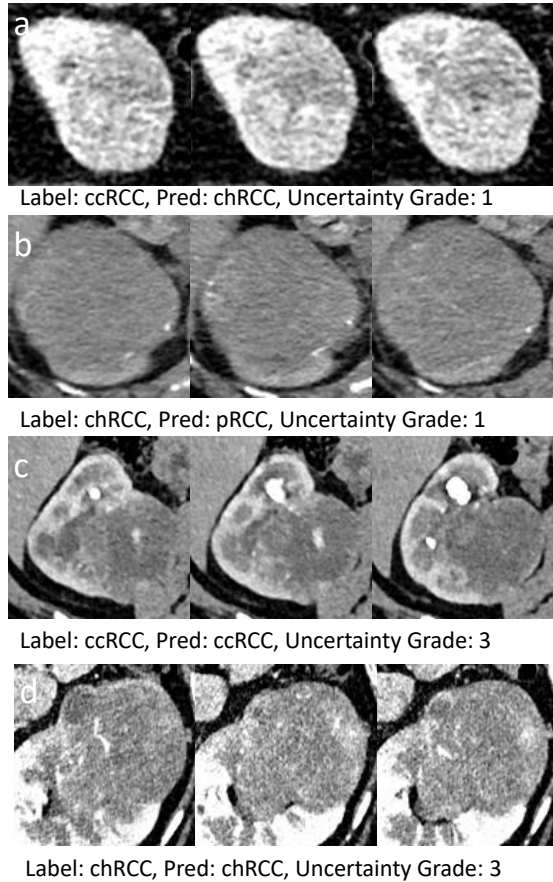


**Fig. 6** Several anomalous cases. CT slices showing cases with low uncertainty but incorrect predictions (a, b) and high uncertainty with correct predictions (c, d). *ccRCC*, clear cell renal cell carcinoma; *pRCC*, papillary renal cell carcinoma; *chRCC*, chromophobe renal cell carcinoma

## Discussion

The ability to accurately classify the pathological subtypes of RCC holds profound implications for patient management and therapeutic strategies. In clinical practice, though the accuracy of deep learning-based diagnostic tools is necessary, it is not sufficient. If a model only provides predictions without indicating its uncertainty, it can mislead radiologists especially when diagnosing intractable diseases[21]. This omission can result in radiologists overlooking the need for further tests, potentially impacting patient diagnosis and treatment. In response to this, our study introduces a deep learning-based model for RCC subtype classification. This model not only provides promising accuracy but also incorporates an uncertainty estimate to determine the model's confidence in its predictions.

Incorporating uncertainty in our model distinctly contrasts with traditional models which often provide a sole classification in medical imaging[22–24]. Such an approach can lead to an overreliance on the model, potentially resulting in misdiagnoses, especially when RCC subtypes have similar phenotypic manifestations. Our method not only offers classification but also sheds light on the model's confidence in its prediction. This dual-output offers a new dimension to clinical practice,

giving clinicians a more comprehensive understanding of the RCC subtype prediction, thereby aiding in more informed decisions. Moreover, by presenting both the subtype prediction and its associated uncertainty, the model effectively reduces the manual evaluation burden on clinicians. This streamlined process not only makes the diagnostic procedure more efficient but also bolsters the clinician's confidence in adopting the model's recommendations, thereby striking a balance between automation and human expertise.

In our results, a lower uncertainty grade was consistently associated with higher correct rates, a trend also observed in the works of Song et al.[25] and Ahsan et al.[26]. This demonstrates the advantage of incorporating uncertainty estimation to enhance diagnostic performance. At the lowest uncertainty grade (grade 1), the correct rate for the internal validation set reached 89.29%, and for the external validation set, 77.78%. Thiagarajan et al.[27] employed a low-dimensional visualization techniques and observed that the low uncertainty images revealed distinct class separations, a manifestation of high classification confidence, reinforcing our own observations. However, at the highest uncertainty grade (grade 5), the correct rate for both validation sets dropped to 0. Research by Rączkowska et al suggests that images with the highest grades of uncertainty often display features that are pathologically challenging to classify[28], providing a potential explanation for our observations. Analyzing the data by subtype, the model performed best for chRCC with correct rates of 94.12% for the internal validation set and 87.50% for the external validation set at grade 1. For pRCC, the rates were 87.5% and 80%, respectively. In contrast, the performance for ccRCC at grade 1 was lower, even though it showed the highest AUC among the three subtypes. One potential factor contributing to this could be the weight settings introduced during model training. Intended to balance the influence of each subtype, the weight adjustments might have unintentionally increased prediction uncertainty for ccRCC. Specifically, the reduced weight for ccRCC, despite its larger dataset, could have made the model more cautious in its predictions for this subtype. This cautiousness might manifest as higher uncertainty, particularly when the model encounters ccRCC cases that resemble to other subtypes.

Our deep learning model exhibited robust performance across diverse RCC subtypes and validation sets, demonstrating its potential reliability for clinical deployment. While deep learning has been extensively applied in medical imaging, research specifically targeting RCC subtype classification is sparse. Most existing studies primarily focus on distinguishing between benign and malignant tumors, or broader classifications such as differentiating ccRCC from non-ccRCC[29]. Traditionally, RCC classifications have been largely dependent on machine learning methods, which often required significant manual oversight, spanning from data preprocessing to feature extraction[30, 31]. In contrast, our model provides an end-to-end solution, substantially reducing the need for human intervention, enhancing the model's applicability in practice through uncertainty estimation, and serving as a significant step towards the clinical application of automated RCC pathological subtypes diagnosis using deep learning.

Our study has several limitations. First, our study was intended to use CT images from the CMP, variations in scanning delays occasionally yielded images that leaned toward PCP or NP. The inclusion of these non-ideal images could potentially influence the model's performance, given that deep learning outcomes are closely tied to the quality and consistency of the training data. Second,

while we introduced a measure of reliability by estimating uncertainty, the "black box" nature of deep learning models remains a challenge to interpret. Third, to mitigate data imbalance, we adjusted weights based on the size of each class. While a common approach, this might have unintentionally affected the model's confidence. Last, our research primarily focuses on a specific imaging modality. Future work could benefit from incorporating diverse modalities, such as MRI and histology images, to further enhance our model's diagnostic capabilities.

### **Conclusion**

In this study, we developed a deep learning model for pathological classification of RCC, providing valuable support to radiologists. The integration of uncertainty estimates enhances the model's transparency and reliability. Future work will focus on refining the uncertainty estimation mechanism and incorporating multi-modal medical data for improved performance.

**Funding** This study received support from the National Natural Science Foundation of China (Grant Numbers: 62106233, 62303427, and 82370513), and the Henan Science and Technology Development Plan (Grant Number: 232102210010, 232102210062, 232102211003, and 222102210219).

### **Declarations**

**Guarantor** The scientific guarantor of this publication is Li Tian.

**Conflict of Interest** The authors of this manuscript declare no relationships with any companies whose products or services may be related to the subject matter of the article.

**Statistics and Biometry** No complex statistical methods were necessary for this paper.

**Informed Consent** Written informed consent was waived by the institutional review board.

**Ethical Approval** Institutional review board approval was obtained.

**Study subjects or cohorts overlap** Study subjects or cohorts have not been previously reported.

### **Methodology**

- Retrospective
- Diagnostic or prognostic study
- Multicenter study

### **References**

1. Ghidini M, Petrelli F, Ghidini A, et al (2017) Clinical development of mTor inhibitors for renal cancer. *Expert Opin Investig Drugs* 26:1229–1237. <https://doi.org/10.1080/13543784.2017.1384813>
2. Liu H, Cao H, Chen L, et al (2022) The quantitative evaluation of contrast-enhanced ultrasound

in the differentiation of small renal cell carcinoma subtypes and angiomyolipoma. *Quant Imaging Med Surg* 12:106–118. <https://doi.org/10.21037/qims-21-248>

3. Robila V, Kraft AO, Smith SC (2019) New entities, new technologies, new findings: A review of the cytologic features of recently established subtypes of renal cell carcinoma. *Cancer Cytopathol* 127:79–97. <https://doi.org/10.1002/cncy.22093>
4. Ghali F, Patel SH, Derweesh IH (2019) Current Status of Immunotherapy for Localized and Locally Advanced Renal Cell Carcinoma. *J Oncol* 2019:7309205. <https://doi.org/10.1155/2019/7309205>
5. Berquist SW, Yim K, Ryan ST, et al (2019) Systemic therapy in the management of localized and locally advanced renal cell carcinoma: Current state and future perspectives. *Int J Urol* 26:532–542. <https://doi.org/10.1111/iju.13943>
6. Yunker A, Holder L, Nething J (2020) Newly described eosinophilic, solid and cystic renal cell carcinoma: a case report and review of the literature. *Archives of Nephrology and Urology* 3:38–45. <https://doi.org/10.26502/anu.2644-2833019>
7. Rasmussen R, Sanford T, Parwani AV, Pedrosa I (2022) Artificial Intelligence in Kidney Cancer. American Society of Clinical Oncology Educational Book 300–310. [https://doi.org/10.1200/EDBK\\_350862](https://doi.org/10.1200/EDBK_350862)
8. Tian L, Li Z, Wu K, et al (2023) The clinical significance of computed tomography texture features of renal cell carcinoma in predicting pathological T1–3 staging. *Quant Imaging Med Surg* 13:2415–2425. <https://doi.org/10.21037/qims-22-1043>
9. Uhm K-H, Jung S-W, Choi MH, et al (2021) Deep learning for end-to-end kidney cancer diagnosis on multi-phase abdominal computed tomography. *npj Precis Onc* 5:54. <https://doi.org/10.1038/s41698-021-00195-y>
10. Kaur R, Juneja M, Mandal AK (2019) Computer-aided diagnosis of renal lesions in CT images: a comprehensive survey and future prospects. *Computers & Electrical Engineering* 77:423–434. <https://doi.org/10.1016/j.compeleceng.2018.07.024>
11. Comes MC, Fucci L, Mele F, et al (2022) A deep learning model based on whole slide images to predict disease-free survival in cutaneous melanoma patients. *Sci Rep* 12:20366. <https://doi.org/10.1038/s41598-022-24315-1>
12. Suarez-Ibarrola R, Hein S, Reis G, et al (2020) Current and future applications of machine and deep learning in urology: a review of the literature on urolithiasis, renal cell carcinoma, and bladder and prostate cancer. *World J Urol* 38:2329–2347. <https://doi.org/10.1007/s00345-019-03000-5>
13. Hussain MA, Hamarneh G, Garbi R (2021) Learnable image histograms-based deep radiomics for renal cell carcinoma grading and staging. *Comput Med Imaging Graph* 90:101924. <https://doi.org/10.1016/j.compmedimag.2021.101924>
14. Toda N, Hashimoto M, Arita Y, et al (2022) Deep Learning Algorithm for Fully Automated Detection of Small ( $\leq 4$  cm) Renal Cell Carcinoma in Contrast-Enhanced Computed Tomography Using a Multicenter Database. *Invest Radiol* 57:327–333. <https://doi.org/10.1097/RLI.0000000000000842>
15. Yang E, Kim CK, Guan Y, et al (2022) 3D multi-scale residual fully convolutional neural network for segmentation of extremely large-sized kidney tumor. *Comput Methods Programs Biomed*

215:106616. <https://doi.org/10.1016/j cmpb.2022.106616>

16. Sun P, Mo Z, Hu F, et al (2023) 2.5D MFPAU-Net: a convolutional neural network for kidney segmentation. *BMC Med Inform Decis Mak* 23:92. <https://doi.org/10.1186/s12911-023-02189-1>
17. Xi IL, Zhao Y, Wang R, et al (2020) Deep Learning to Distinguish Benign from Malignant Renal Lesions Based on Routine MR Imaging. *Clin Cancer Res* 26:1944–1952. <https://doi.org/10.1158/1078-0432.CCR-19-0374>
18. Han S, Hwang SI, Lee HJ (2019) The Classification of Renal Cancer in 3-Phase CT Images Using a Deep Learning Method. *J Digit Imaging* 32:638–643. <https://doi.org/10.1007/s10278-019-00230-2>
19. Wang X, Deng X, Fu Q, et al (2020) A Weakly-Supervised Framework for COVID-19 Classification and Lesion Localization From Chest CT. *IEEE Trans Med Imaging* 39:2615–2625. <https://doi.org/10.1109/TMI.2020.2995965>
20. Sensoy M, Kaplan L, Kandemir M Evidential Deep Learning to Quantify Classification Uncertainty
21. Seoni S, Jahmunah V, Salvi M, et al (2023) Application of uncertainty quantification to artificial intelligence in healthcare: A review of last decade (2013–2023). *Computers in Biology and Medicine* 165:107441. <https://doi.org/10.1016/j.combiomed.2023.107441>
22. Yu Q, Ning Y, Wang A, et al (2023) Deep learning–assisted diagnosis of benign and malignant parotid tumors based on contrast-enhanced CT: a multicenter study. *Eur Radiol* 33:6054–6065. <https://doi.org/10.1007/s00330-023-09568-2>
23. Panthakkan A, Anzar SM, Jamal S, Mansoor W (2022) Concatenated Xception-ResNet50 - A novel hybrid approach for accurate skin cancer prediction. *Comput Biol Med* 150:106170. <https://doi.org/10.1016/j.combiomed.2022.106170>
24. Yang X, Xi X, Yang L, et al (2022) Multi-modality relation attention network for breast tumor classification. *Comput Biol Med* 150:106210. <https://doi.org/10.1016/j.combiomed.2022.106210>
25. Song B, Sunny S, Li S, et al (2021) Bayesian deep learning for reliable oral cancer image classification. *Biomed Opt Express* 12:6422–6430. <https://doi.org/10.1364/BOE.432365>
26. Ahsan MA, Qayyum A, Razi A, Qadir J (2022) An active learning method for diabetic retinopathy classification with uncertainty quantification. *Medical & Biological Engineering & Computing* 60:2797–2811. <https://doi.org/10.1007/s11517-022-02633-w>
27. Thiagarajan P, Khairnar P, Ghosh S (2022) Explanation and Use of Uncertainty Quantified by Bayesian Neural Network Classifiers for Breast Histopathology Images. *IEEE Transactions on Medical Imaging* 41:815–825. <https://doi.org/10.1109/TMI.2021.3123300>
28. Rączkowska A, Możejko M, Zambonelli J, Szczerk E (2019) ARA: accurate, reliable and active histopathological image classification framework with Bayesian deep learning. *Scientific Reports* 9:14347. <https://doi.org/10.1038/s41598-019-50587-1>
29. Shehata M, Alksas A, Abouelkheir RT, et al (2021) A Comprehensive Computer-Assisted Diagnosis System for Early Assessment of Renal Cancer Tumors. *Sensors (Basel)* 21: <https://doi.org/10.3390/s21144928>
30. Kocak B, Yardimci AH, Bektas CT, et al (2018) Textural differences between renal cell carcinoma subtypes: Machine learning-based quantitative computed tomography texture analysis with

independent external validation. Eur J Radiol 107:149–157.  
<https://doi.org/10.1016/j.ejrad.2018.08.014>

31. Uhlig J, Leha A, Delonge LM, et al (2020) Radiomic Features and Machine Learning for the Discrimination of Renal Tumor Histological Subtypes: A Pragmatic Study Using Clinical-Routine Computed Tomography. *Cancers (Basel)* 12:. <https://doi.org/10.3390/cancers12103010>